Improved Methods for Hydrofrac Event Detection and Phase Picking

Fuxian Song, H. Sadi Kuleli, M. Nafi Toksoz, and Haijiang Zhang, Massachusetts Institute of Technology, Bruce Cornish, John Quirein, Erkan Ay, Donghong Pei and Steve Zannoni, Halliburton Energy Services Company*

Summary

The ability to detect small microseismic events and identify their P and S phase arrivals is a key issue in hydraulic fracture monitoring because of the low signal-to-noise ratios. We propose a array-based waveform correlation approach to detect small magnitude events with similar mechanisms and locations as a nearby master event. For the phase picking part, a transformed spectrogram method is used to identify the weak P arrivals. We have applied the technique to a downhole monitoring dataset of the microseismic events induced by hydraulic fracturing. The results show a better phase identification.

Introduction

Unconventional oil and gas reservoirs like tight gas reservoirs are problematic to produce, often requiring multiple stages of hydraulic fracturing in order to create connected pathways through which hydrocarbons may flow. During hydrofrac treatment, many induced earthquakes occur along the maximum horizontal stress direction and reactivated pre-existing fractures. These induced microseismic events are extremely important in terms of evaluating the effectiveness of hydraulic fracturing operations. Their locations are typically used to derive the fracture plane orientation which is then used to optimize the late-stage treatment. However, typically these are small events, which are hard to detect and locate. In this study, we propose a systematic approach to detect these small events and identify their phase arrivals.

In earthquake seismology, waveform correlation of strong events known as master events is used to detect weaker events (e.g. Yang et al. 2003, Gibbons and Ringdal, 2006). A similar

method is also used in reflection seismology, where a complex source-time function, known as chirp or sweep, is used as a matched filter to reconstruct Green's functions between sources and receivers (e.g. Yilmaz, 1987). These correlation based detectors are especially useful to lower the detection threshold. In this study we adapt it to hydrofrac monitoring setup by building a master event library in real time and using them as our cross-correlation template to detect small events which share a similar location, fault mechanism and propagation path with master events.

Following event detection, a robust approach is needed to identify their P & S arrivals. Typically the STA/LTA type of picking algorithm is used to identify P & S arrival times (e.g. Earle and Shearer, 1994). The problem with the STA/LTA method is that it is very sensitive to background noise level, which can be an issue in hydraulic fracturing. For noisy hydrofrac dataset, STA/LTA pickings can be very erroneous especially for the weak P phases. Here, we propose a transformed spectrogram based approach which can eliminate the influence of high background noise.

Methodology

The seismic waveforms observed at any receiver can be modeled as a convolution of the source, medium and receiver response (e.g. Stein, and Wysession, 2002):

$$D(t) = S(t) \otimes G(t) \otimes R(t) \tag{1}$$

Where $D(t)$ is the recorded seismic data, $S(t), G(t)$ and $R(t)$ represent source wavelet, medium Green's function and receiver response respectively. Thus, two nearby events sharing similar source mechanism and source location will show similar waveforms observed at the same receiver. This is the basis for the cross-correlation detector. Once a master event with a good signal-to-noise ratio is identified, it can be used as a template to cross correlate with the whole noisy record. A high cross-correlation coefficient indicates the arrival of a microseismic event. A simple threshold for the cross-correlation coefficient constructs an efficient small event detector.

A further advantage of this detection method for multi-stage hydrofrac job is that the master event can be updated in real time to capture the fracture propagation.

Following the event detection, an unbiased, stable and high-resolution multi-taper based spectrogram estimate of the recorded data is obtained to both validate previous detection results and to further identify the phase arrivals. The basic idea of the multi-taper spectrogram is that the conventional spectral analysis method suppresses the spectral leakage by tapering the data before Fourier transforming (e.g. Percival et al. 1993). This is equivalent to discarding data far from the center of the time series. Any statistical estimation procedure which literally throws away data is unlikely to be a very sensible one, because real information is being discarded. So the multi-taper method begins by constructing a series of N orthogonal tapers, and then applies the tapers to the original data to obtain N sets of tapered data. Because of the orthogonality of the tapers, there will be a tendancy for the N sets of tapered data to be nearly uncorrelated. If the underlying process is near-Gaussian, those N sets of tapered data will therefore be nearly independent. Thus the sum of Fourier transforms of these N sets of tapered data will give us an unbiased, stable and high-resolution spectral estimate. The multi-taper spectrogram is then differentiated with respect to time to eliminate the background noise. A transformed spectrogram is then formed by multiplying the differentiated spectrogram with the original spectrogram to highlight two features of a phase arrival: high energy contrast and high energy (e.g. Gibbons, Ringdal and Kvaerna, 2008). Mathematically speaking, let the spectrogram estimate within time window [t, t+L] be denoted by $A(f,t,L)$, the transformed spectrogram can be expressed as:

$$S(f,t) = (\log_{10}[A(f,t,L)] - \log_{10}[A(f,t-L,L)])\log_{10}[A(f,t,L)] \quad (2)$$

The characteristic function of this transformed spectrogram can be defined over signal frequency range $[f_1 : f_2]$ as:

$$\bar{S}([f_1 : f_2],t) = \frac{1}{N_f}\sum_{f=f_1}^{f_2} S(f,t) \quad (3)$$

Where N_f is the number of frequency points over the signal frequency range $[f_1 : f_2]$. The P & S arrivals can then be readily identified as two peaks in this characteristic function.

Field Data Example

A microseismic monitoring survey was performed during a hydraulic fracturing job in 2008. The microseismic data was recorded in a monitoring well with a 7-geophone tool during the treatment. Figure 1 shows one recording of 32s. Noise and signal spectrum analysis show a dominant signal frequency from 75 Hz up to 300 Hz. A bandpass filter of [75 300] Hz was applied to the raw data to get an enhanced signal as shown in Figure 2. From bandpass filtered data in Figure 2, three major microseismic events around 8.25s, 19.25s and 27.98s can be seen and detected by the standard STA/LTA event detection and picking algorithm. The event around 19.25s as shown in Figure 3 is selected as the master event, which includes both P and S arrivals. As an example, Figure 4 a) shows the bandpass filtered data from geophone 2, where the master event is shown as '#'. Figure 4 b) gives the correlation detector output using only one geophone and Z component data. Besides these three big events, we also see a clear event around 13.5s in Fig. 4 b) marked as '*', where the correlation detector output has a peak. This event is barely identifiable by the standard detection algorithms, since its amplitude is at the noise level. We also see a very likely event around 2.28s shown as '&' in Fig. 4 b), which is identifiable but not so obvious. Figure 4 c) and d) represent the array-stacked correlation detection results with all 7 geophones. Figure 4 c) uses only Z component, while Figure 4 d) utilizes all 3 components. From these two figures, it is easy to identify the '&' event. The correlation detection result in Figure 4 d), which utilizes all 3 components, has the highest signal-to-noise ratio compared to Figure 4 c) and b). Three factors including waveform matching, cross-geophone stacking and matching in polarization structure contribute to the processing gain for the 3-component array-based correlation detector. This shows that 3-component array-based correlation detector is very sensitive to small-magnitude events especially under the Gaussian noise environment.

Once an event is detected, the next step is to use a multi-taper based transformed spectrogram approach to identify the P and S arrivals associated with this event. Figure 5 a) gives the bandpass filtered data from geophone 2. Figure 5 b) and c) represents the transformed spectrogram $S(f,t)$ of the bandpass filtered data and its characteristic function $\bar{S}([75:300],t)$ respectively. Five events are clearly shown in both figures. This further validates our correlation detection results. To pick P and S arrivals, the zoomed version of the characteristic function $\bar{S}([75:300],t)$ around the master event together with its bandpass filtered waveform is shown in Figure 6 a) and b). In Figure 6 b), it is easy to pick both P and S arrivals whereas even on the [75, 300] Hz bandpass filtered waveform, the P arrival is still hard to pick due to its low signal-to-noise ratio. This shows that our transformed spectrogram as shown in the equations (2), (3) can enhance the weak P arrivals and help to pick these weak arrivals.

We have also tested the above approach with the other 6 geophones for this dataset and several other datasets. The conclusion still holds. Even more promising is that most geophones show better results than geophone 2 which is demonstrated here, because they have a higher signal-to-noise ratio as seen in Figure 2.

Conclusions

In this paper, we have proposed a systematic approach for hydrofrac event detection and phase picking. By field test, we have demonstrated that a cross-correlation detection method using master event can effectively increase our capability to detect small nearby events. Also we have shown that the transformed spectrogram and its characteristic function can help us both detect small events and pick weak arrivals, since it captures two features of a phase arrival in the time-frequency domain: high energy and high energy increase.

Acknowledgements

The authors would like to thank the Halliburton Energy Services Company Houston office for their help in providing the data and the financial support, and the management of Halliburton for permission to publish this work.

Reference

Earle, P.S., and Shearer, P.M., 1994, Characterization of global seismograms using an automatic-picking algorithm: Bulletin of the Seismological Society of America, **84**, 366-376.

Gibbons, S. J., and Ringdal F., 2006, The detection of low magnitude seismic events using array-based waveform correlation: Geophysical Journal International, **165**, 149–166.

Gibbons, S.J., Ringdal, F., and Kvaerna, T., 2008, Detection and characterization of seismic phases using continuous spectral estimation on incoherent and partially coherent arrays: Geophysical Journal International, **172**, 405-421.

Percival, D. B., and Walden A. T., 1993, Spectral Analysis for Physical Applications. Multitaper and Conventional Univariate Techniques: Cambridge Univ. Press.

Stein, S., and Wysession, M., 2002, An Introduction to Seismology, Earthquakes and Earth Structure:Wiley-Blackwell.

Yang, W., Aster, R., Thurber, C., Young, C., and Hart, D., 2003, Using Waveform Cross-correlation to Detect and Identify Regional Seismic Phases Based on Reference Event Sets: EOS trans. AGU, **84**, 46.

Yilmaz, O., 1987, Seismic data processing investigations in geophysics: SEG.

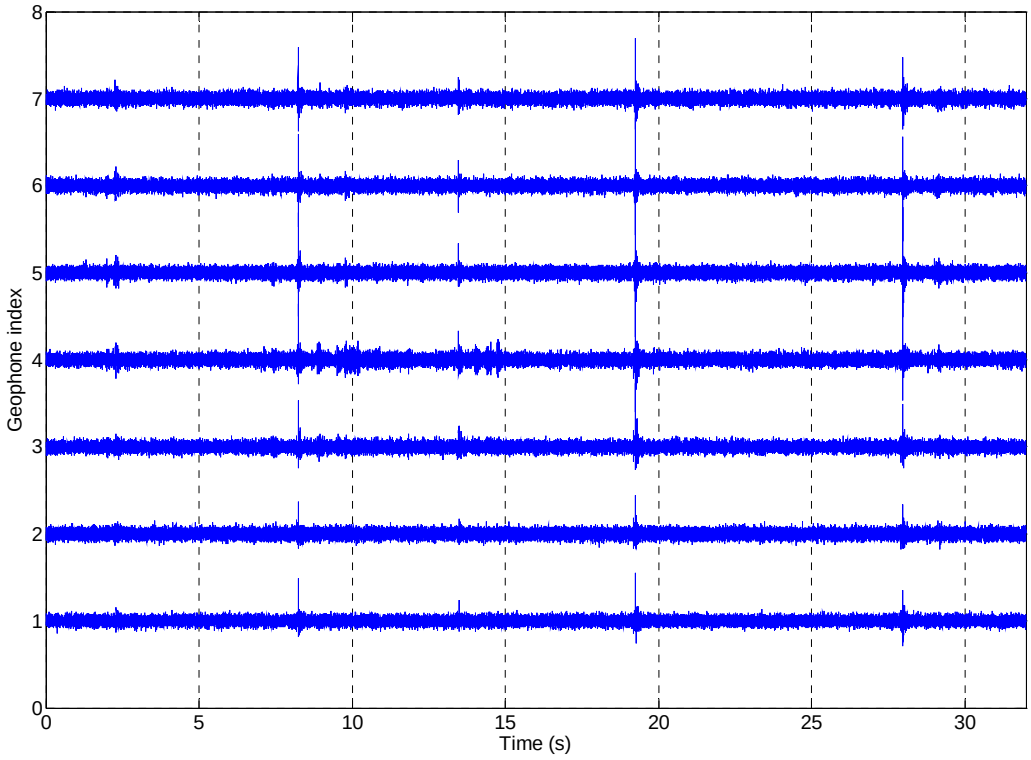

Figure 1: Vertical velocity data recorded by a 10-geophone downhole array

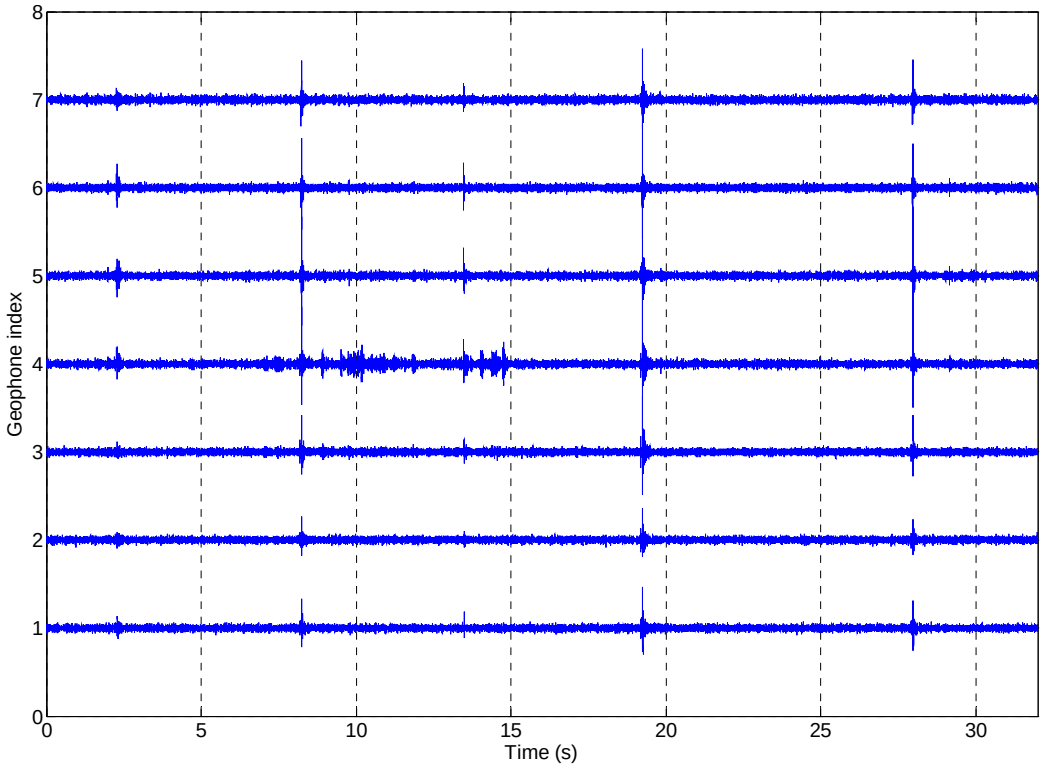

Figure 2: [75 300] Hz band-pass filtered vertical velocity data

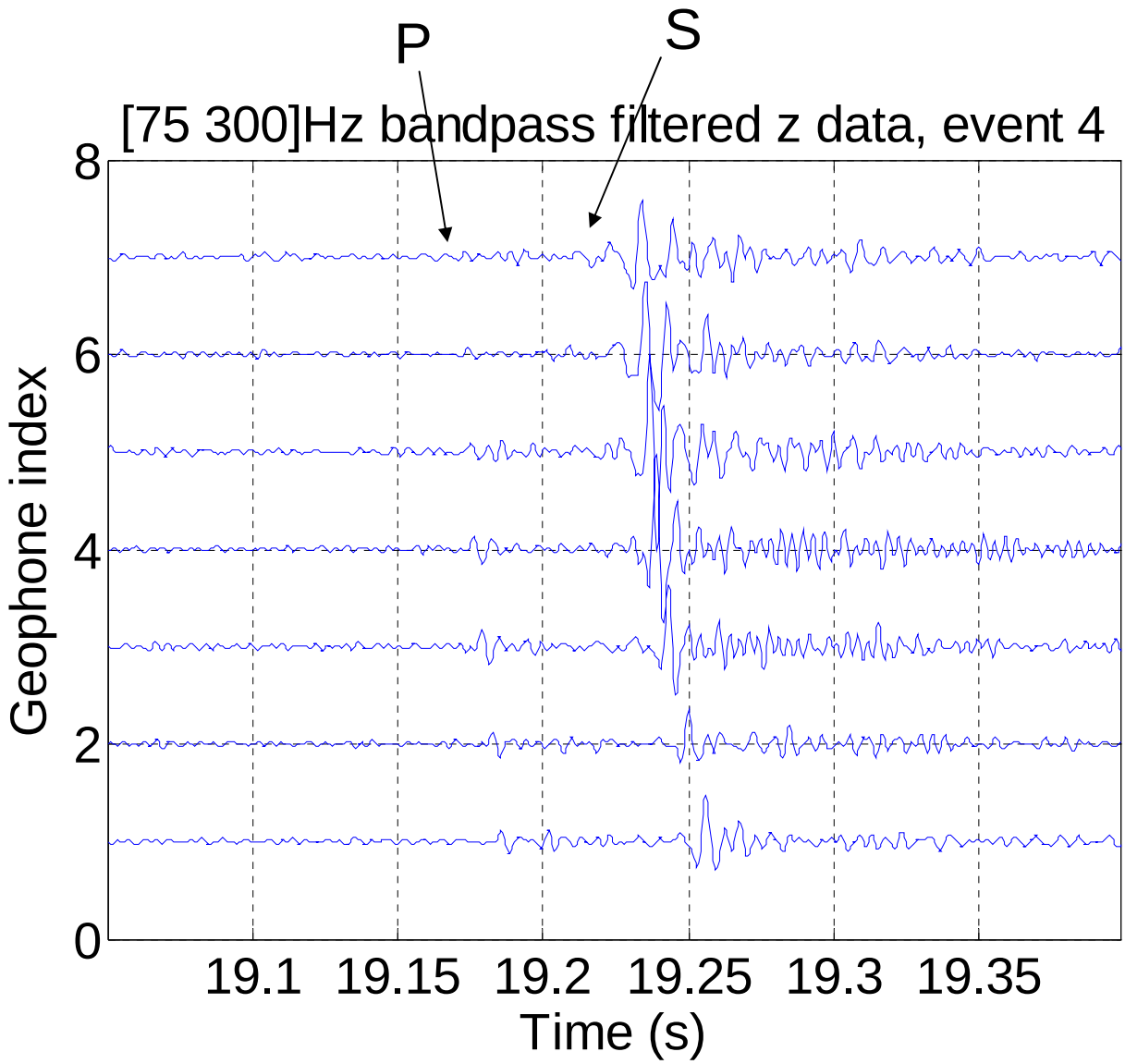

Figure 3: Master event waveform as cross-correlation template

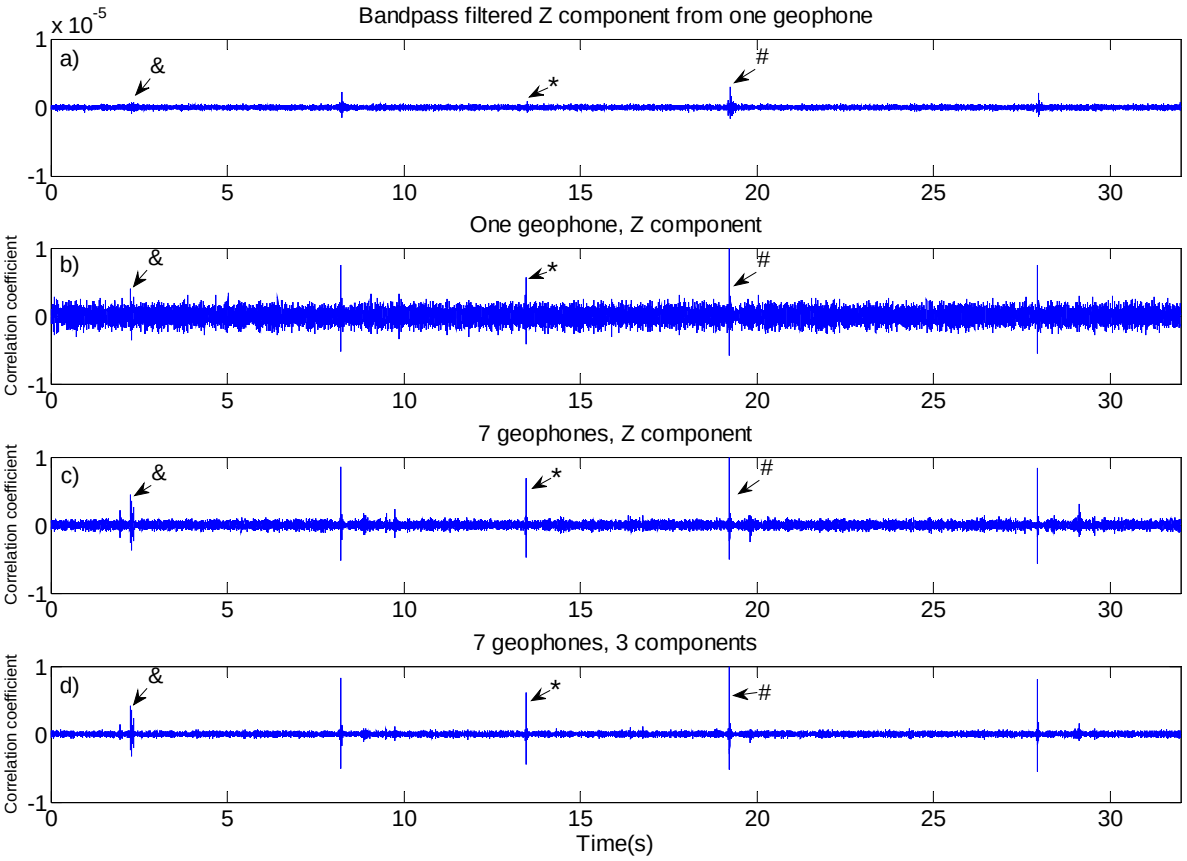

Figure 4: a) [75 300] Hz band-pass filtered vertical velocity from geophone 2, b) waveform correlation detector output using 1 geophone, 1 component, c) waveform correlation detector output using 7 geophones, 1 component, d) waveform correlation detector output using 7 geophones, 3 components (*, &: event not detectable by STA/LTA, #: master event).

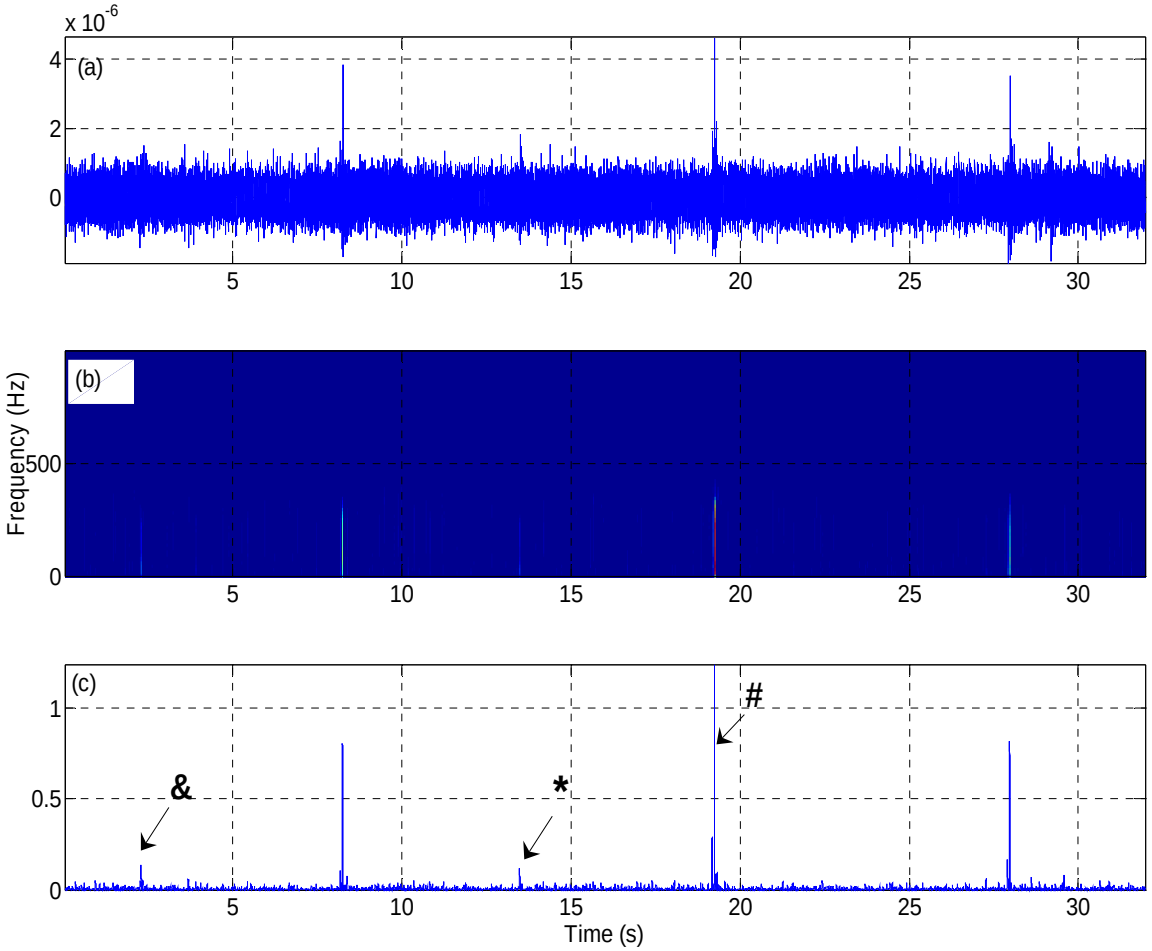

Figure 5: (a) [75 300] Hz band-pass filtered vertical velocity from geophone 2, (b) Transformed spectrogram S(f,t) as shown in equation (2), (c) Characteristic function of the transformed spectrogram Sbar([75:300],t) as specified in equation (3).

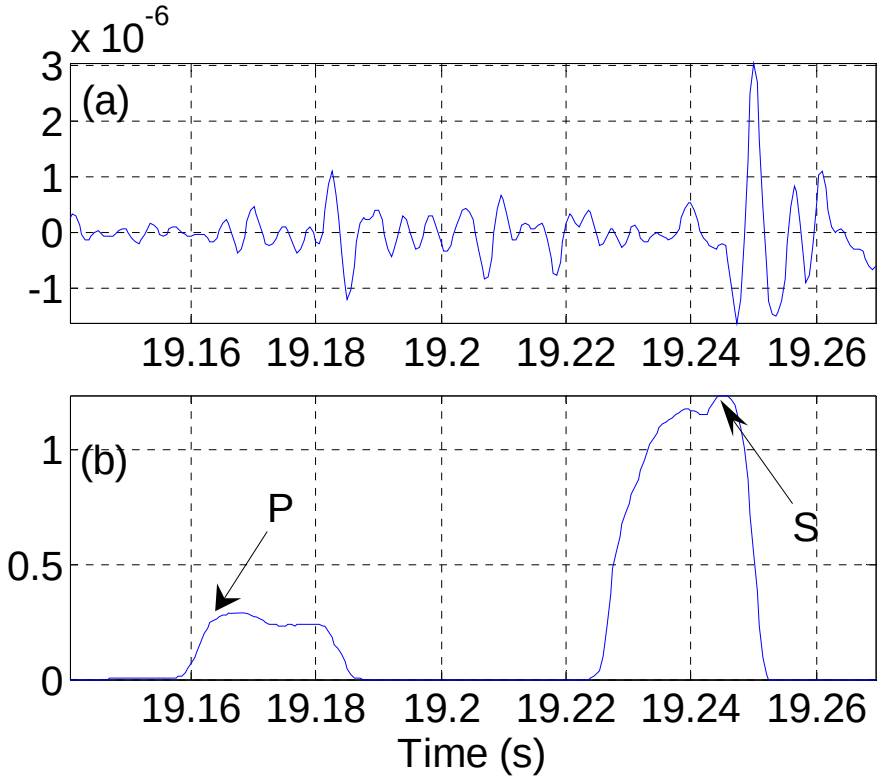

Figure 6: (a) [75 300] Hz band-pass filtered vertical velocity from geophone 2 for the master event, (b) Characteristic function of the transformed spectrogram Sbar([75:300],t) as specified in equation (3) for the master event (P and S arrivals are clearly indentified here).